Charge Transfer through Isomeric Unsaturated Hydrocarbons. Redox Switchable Optical Properties and Electronic Structure of Substituted Indenes with a Pendant Ferrocenyl

Saverio Santi,* Laura Orian, Alessandro Donoli, Christian Durante, Annalisa Bisello, Paolo Ganis, and Alberto Ceccon*

Dipartimento di Scienze Chimiche, Università degli Studi di Padova, via Marzolo 1, 35131 Padova, Italy

Laura Crociani and Franco Benetollo

CNR, Istituto di Chimica Inorganica e delle Superfici, Corso Stati Uniti 4, 35127 Padova, Italy

Received July 5, 2007

A family of (ferrocenyl)indenes, (2-ferrocenyl)indene, (2-ferrocenyl)tetramethylindene, (2-ferrocenyl)-hexamethylindene, (3-ferrocenyl)indene, and (3-ferrocenyl)hexamethylindene, and the corresponding monooxidized cations have been prepared. The results of a structural and spectroelectrochemical study are discussed. The availability of pairs of isomers with known geometries and differently methylated indenes allowed the detailed investigation of how slight geometric and electronic modifications affect their physical properties. The molecular structures have been determined by X-ray diffraction and compared with the fully optimized structures calculated with state-of-the-art DFT methods. Calculated and crystallographic structures agree in establishing the dependence of the orientation of the indene moiety and the ferrocenyl cyclopentadienyl rings on the degree of methylation. The UV−vis spectra and in particular the appearance upon oxidation of a new near-IR absorption, whose energy and intensity increase with the degree of methylation and cyclopentadienyl-indene planarity, are rationalized in the framework of the Hush theory and at quantum chemistry level by DFT and TD-DFT calculations.

Introduction

Metal-containing conjugated systems have emerged as an important category of materials.[1] The impetus for developing these materials is based on the premise that conjugated hydrocarbons containing metals are expected to possess properties significantly different from those of conventional organic conjugated molecules. Examples of these properties include electrical conductivity,[2] magnetic behavior,[3] luminescence,[4] and nonlinear optical (NLO) effects.[5]

Ferrocenyl-conjugated molecules are attracting much interest since they can be used as building blocks for the synthesis of (poly)ferrocenyl-conjugated systems[6] or as starting material for preparing novel heterobimetallic[7] donor−acceptor complexes with unusual properties. In addition, ferrocenyl-conjugated derivatives represent suitable models for the study of the electronic communication between terminal subunits in terms of tuning the electron properties and the reactivity of materials.[6−8] Finally, the ferrocenyl unit possesses high chemical stability in both the neutral and oxidized states, chemical reversible redox behavior, and ease of functionalization.[9] For these reasons, the π-conjugated systems formed by the iron-coordinated cyclopentadienyl (Cp) ring and its aromatic substituent associated with the redox switchable electron donor/acceptor capability of the ferrocene/ferrocenium couple are expected to display attractive electronic and optical properties that depend on the

(1) (a) Holliday, B. J.; Swager, T. M. *Chem. Commun.* **2005**, 23−36. (b) Wolf, M. O. *J. Inorg. Organomet. Polym. Mater.* **2006**, *16*, 189−199. (c) Stott, T. L. Wolf, M. O. *Coord. Chem. Rev.* **2003**, *246*, 89−101.

(2) Shirakawa, H. *Angew. Chem., Int. Ed.* **2001**, *40*, 2574−2580.

(3) Miller, J. S.; Epstein, A. J. *Angew. Chem., Int. Ed. Engl.* **1994**, *33*, 385−415.

(4) Fery-Forgues, S.; Delavaux-Nicot, B. *J. Photochem. Photobiol. A: Chem.* **2000**, *132*, 137−159.

(5) (a) Zheng, Q.; He, G. S.; Lu, C.; Prasad, P. N. *J. Mater. Chem.* **2005**, *15*, 3488−3493. (b) Powell, C. E.; Humphrey *Coord. Chem. Rev.* **2004**, *248*, 725−756. (c) Barlow, S.; Marder, S. R. *Chem. Commun.* **2000**, 1555−1562. (d) Di Bella, S. *Chem. Soc. Rev.* **2001**, *30*, 355−366. (e) Heck, J.; Dabek, S.; Meyer-Friedrichsen, T.; Wong, H. *Coord. Chem. Rev.* **1999**, *190−192*, 1217−1254.

(6) (a) Debroy, P.; Roy, S. *Coord. Chem. Rev.* **2007**, *251*, 203−221. (b) Lim, Y.-K.; Wallace, L.; Bollinger, J. C.; Chen, X.; Lee, D. *Inorg. Chem.* **2007**, *46*, 1694−1703. (c) Chebny, V. L.; Dhar, D.; Lindeman, S. V.; Rathore, R. *J. Org. Chem.* **2006**, *8*, 5041−5044. (d) Yu, Y.; Bond, A. D.; Leonard, P. W.; Lorenz, U. J.; Timofeeva, T. V.; Vollhardt, K. P. C.; Whitener, G. D.; Yakovenko, A. A. *Chem. Commun.* **2006**, 2572−2574. (e) Vives. G.; Carella, A.; Launay, J.-P.; Rapenne, G. *Chem. Commun.* **2006**, 2283−2285. (f) Yu, Y.; Bond, A. D.; Leonard, P. W.; V.; Vollhardt, K. P. C.; Whitener, G. D. *Angew. Chem., Int. Ed.* **2006**, *45*, 1794−1799.

(7) (a) Ceccon, A.; Santi, S.; Orian, L.; Bisello, A. *Coord. Chem. Rev.* **2004**, *248*, 683−724. (b) Warratz, R.; Peters, G.; Studt, F.; Römer, R.-H.; Tuczek, F. *Inorg. Chem.* **2006**, *45*, 2531−2542. (c) Szesni, N.; Drexler, M.; Maurer, J.; Winter, R. F.; de Montigny, F., Lapinte, C.; Steffens, S.; Heck, J.; Weibert, B.; Fischer H. *Organometallics* **2006**, *25*, 5774−5787. (d) Gaede, P. E.; van Wullen, C. *Z. Anorg. Allg. Chem.* **2006**, *632*, 541−552. (e) Li, M.; Riache, N.; Tranchier, J.-P.; Rose-Munch, F.; Rose, E.; Herson, P.; Bossi, A.; Rigamonti, C.; Licandro, E. *Synthesis* **2007**, 277−283.

(8) (a) Low, P. J.; Roberts, R. L.; Cordiner, R. L.; Hartl, F. *J. Solide State Electrochem.* **2005**, *9*, 717−731. (b) Jiao, J.; Long, G. J.; Rebbouh, L.; Grandjean, F.; Beatty, A. M.; Fehlner, T. P. *J. Am. Chem. Soc.* **2005**, *127*, 17819−17831. (c) Xu, G.-L.; Crutchley, R. J.; DeRosa, M. C.; Pan, Q.-J.; Zhang, H.-X.; Wang, X. P.; Ren, T. *J. Am. Chem. Soc.* **2005**, *127*, 13354−13363. (d) Jones, S. C.; Barlow, S.; O'Hare, D. *Chem.−Eur. J.* **2005**, *11*, 4473−4481. (e) Barlow, S.; O'Hare, D. *Chem. Rev.* **1997**, *97*, 637−670. (f) Ribou, A.-C.; Launay, J.-P.; Sachtleben, M. L.; Li, H.; Spangler, C. W. *Inorg. Chem.* **1996**, *35*, 3735−3740. (g) Tolbert, L. M.; Zhao, X.; Ding, Y.; Bottomley, L. A. *J. Am. Chem. Soc.* **1995**, *117*, 12891−12892.

(9) A special issue was dedicated to ferrocene and its derivatives: *J. Organomet. Chem.* **2001**, *637*−639, 1−875.

10.1021/om700673m CCC: $37.00
Publication on Web 10/23/2007

Scheme 1. Synthesis of 1−5 Starting from Ferrocenyl Lithium and the Corresponding 2- and 3-Indanones

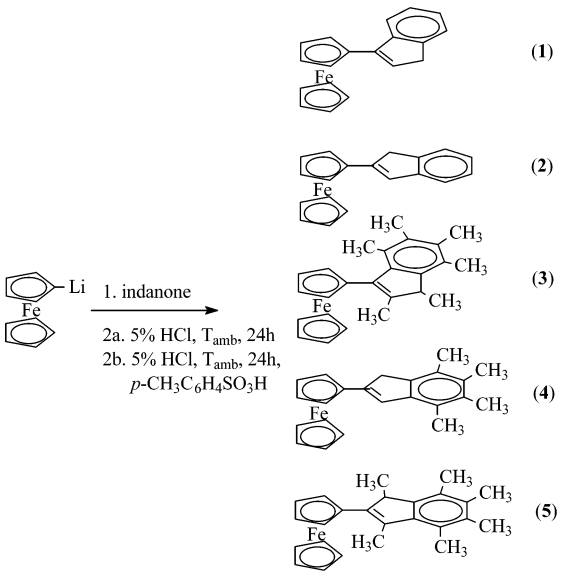

nature and disposition of the organic substituent and on the redox state of the pendant ferrocenyl.

Understanding and control of electron and energy transfer processes both in mono- and in bimetallic complexes is of great importance since the knowledge of the factors that influence the mechanistic pathway is crucial for theoretical investigations and practical applications. In particular, in the class of mixed-valence bimetallic species formed by oxidation of one metal unit the magnitude of the electronic coupling is largely dependent on the structure and stereochemistry of the bridging ligand[7a,8e,10] and increases if the spacer is forced to adopt a planar geometry.[11] For instance, we have recently shown that the interaction between iron and chromium[12] and iron and rhodium[13] strongly depends on the geometry of the bridging ligand. In fact, the electronic coupling between iron and chromium in the mixed-valence ions of the two isomers [η^6-(2-ferrocenyl)indene]-$Cr(CO)_3$ and [η^6-(3-ferrocenyl)indene]$Cr(CO)_3$ is more pronounced in the former due to the almost coplanarity (torsion angle value 10°) of the indenyl and cyclopentadienyl moieties in the bridging ligand. In contrast, such planarity is lost in the 3-isomer, where the torsion angle is 31°. Similarly, in the pair of mixed-valence isomer cations [η^5-(2-ferrocenyl)indene]Rh-$(cod)^+$ and [η^5-(3-ferrocenyl)indenyl]$Rh(cod)^+$ the 2-isomer displays valence delocalization and much stronger coupling than the 3-isomer.

While the charge or energy transfer phenomena in homo- and heterobimetallic mixed-valence complexes have been widely investigated, studies on systems where the ferrocenium is the acceptor of charge or energy from an organic donor have been recently intensified. The aim is the fine-tuning of the donor−acceptor moieties by varying their structural and electronic properties, and in this context numerous aryl ligands have been employed such as phenyl,[14] naphthalene, anthracene, pyrene,[15] fluorene,[16] acridine, acridone, anthraquinone,[17] pyridine,[14,18] and thiophene,[1c,6a,19] directly bonded to the ferrocenyl group or connected by different π-linkages. However, only in a few cases[15a,c,19c] have the results been interpreted in the framework of the classical two-state Hush theory. The indene, which belongs to the class of the olefinic backbones, is the aryl ligand used in the present study. Its main feature is the possibility to be linked to the ferrocene in different positions through its vinyl fragment and to be easily functionalized by methyl groups, thus modulating both its donor and steric properties in the attempt to rationalize the intramolecular charge transfer with the Hush theory.

In fact, upon oxidation of aryl-ferrocenes, the electronic transition of the ferrocenyl in the UV region is typically replaced by ligand-to-metal (LMCT) charge transfer bands in the visible region and in some cases by new bands in the near-IR assigned to aryl → ferrocenium transitions. The goal is to switch on or off the absorption of the near-IR radiation by mean of the ferrocenyl redox couple and to increase the absorption coefficient of the transition by modification of the arene group, the main requisite for technological applications. It has been demonstrated that in an electrochromic system the gap between the oxidation potentials of the metal group and the organic donor end group correlates with a low-energy band in the near-IR; the smaller the gap, the lower the near-IR transition occurs.[20−22] The classical electron transfer Hush model, developed for interpretation of the intervalence charge transfer (IT) bands of bimetallic[21−23] and organic[24] molecules, has been also extended to the LMCT and MLCT transfer processes to get insight into the delocalization in monometallic metal-based conjugated

(10) (a) D'Alessandro, D. M.; Dinolfo, P. H.; Hupp, J. T.; Junk, P.C.; Keene, F. R. *Eur. J. Inorg. Chem.* **2006**, *4*, 772−783. (b) Welter, S.; Brunner, K.; Hofstraat, J. W.; De Cola, L. *Nature* **2003**, *421*, 54−57. (c) Chen, J. Y.; Kao, C.-H.; Lin, S. J.; Tai, C.-C.; Kwan, K. S. *Inorg. Chem.* **2000**, *39*, 189−194.

(11) Benniston, A. C.; Harriman, A. *Chem. Soc. Rev.* **2006**, *35*, 169−179.

(12) Santi, S.; Ceccon, A.; Bisello, A.; Durante, C.; Ganis, P.; Orian, L.; Benetollo, F.; Crociani, L. *Organometallics* **2005**, *24*, 4691−4694.

(13) Santi, S.; Orian, L.; Durante, C.; Bisello, A.; Benetollo, F.; Crociani, L.; Ganis, P.; Ceccon, A. *Chem.−Eur. J.* **2007**, *13*, 1955−1968.

(14) Peris, E. *Coord. Chem. Rev.* **2004**, *248*, 279−297.

(15) (a) Flood, A. H.; McAdam, C. J.; Gordon, K. C.; Kjaergaard, H. G.; Manning, A. M.; Robinson, B. H. Simpson, J. *Polyhedron* **2007**, *26*, 448−455. (b) Martínez, R.; Ratera, I.; Tárraga, A.; Molina, P.; Veciana, J. *Chem. Commun.* **2006**, 3809−3811. (c) Cuffe, L.; Richard, D. A.; Hudson, R. D. A.; Gallagher, G. F.; Jennings, S.; McAdam, C. J.; Connely, R. B. T.; Manning, A. M.; Robinson, B. H. Simpson, J. *Organometallics* **2005**, *24*, 2051−2060. (d) Butler, I. R.; Hobson, L. J.; Coles, S. J.; Hursthouse, M. B.; Abdul Malik, K. M. *J. Organomet. Chem.* **1997**, *540*, 27−40.

(16) Thomas, K. R. J.; Lin, J. T.; Lin, H.-M.; Chang, C.-P.; Chuen, C.-H. *Organometallics* **2001**, *20*, 557−563.

(17) McGale, E. M.; Robinson, B. H. Simpson, J. *Organometallics* **2003**, *22*, 931−939.

(18) Paolucci, D.; Marcaccio, M.; Bruno, C.; Braga, D.; Polito, M.; Paolucci, F.; Grepioni, F. *Organometallics* **2005**, *24*, 1198−1203.

(19) (a) Chen, J.; Burrell, A. K.; Collis, G. E.; Officer, D. L.; Swiegers, G. F.; Too, C. O. Wallace, G. G. *Electrochim. Acta* **2002**, *47*, 2715−2724. (b) Hudson, R. D. A.; Asselberghs, I.; Clays, K.; Cuffe, L. P.; Gallagher, J. F.; Manning, A. R.; Persoons, A.; Wostyn, K. *J. Organomet. Chem.* **2001**, *637−639*, 435−444. (c) Zhu, Y.; Wolf, M. O. *J. Am. Chem. Soc.* **2000**, *122*, 10121−10125. (d) Zhu, Y.; Wolf, M. O. *Chem. Mater.* **1999**, *11*, 2995-3001.

(20) Hush, N. S. *Prog. Inorg. Chem.* **1967**, *8*, 391−444.

(21) Crutchley, R. J. *Adv. Inorg. Chem.* **1994**, *41*, 273−325.

(22) Creutz, C. *Prog. Inorg. Chem.* **1983**, *30*, 1−73.

(23) For a very recent review see: Kaim, W.; Lahiri, G. K. *Angew. Chem., Int. Ed.* **2007**, *46*, 1778−1796, and references therein.

(24) (a) Nelsen, S. F.; Adamus, J.; Wolff, J. J. *J. Am. Chem. Soc.* **1994**, *116*, 1589−1590. (b) Nelsen, S. F.; Trieber, D. A.; Wolff, J. J.; Powell, D. R.; Rogers-Crowley, S. *J. Am. Chem. Soc.* **1997**, *119*, 6873−6882. (c) Lambert, C.; Nöll, G. *J. Am. Chem. Soc.* **1999**, *121*, 8434−8442. (d) Holzapfel, M.; Lambert, C.; Selinka, C.; Stalke, D. *J. Chem. Soc., Perkin Trans. 2* **2002**, 1553−1561. (e) Sun, D.-L.; Rosokha, S. V.; Lindeman, S. V.; Kochi, J. K. *J. Am. Chem. Soc.* **2003**, *125*, 15950−15963. (f) Amthor, S.; Noller, B.; Lambert, C. *Chem. Phys.* **2005**, *316*, 141−152. (g) Amthor, S.; Lambert, C. *J. Phys. Chem. A* **2006**, *110*, 1177−1189. (h) Heckmann, A.; Amthor, S.; Lambert, C. *Chem. Commun.* **2006**, 2959−2961. (i) Nelsen, S. F.; Konradsson, A. E. Teki, Y. *J. Am. Chem. Soc.* **2006**, *128*, 2902−2910.

Scheme 2. Synthesis of Methylated 2-Indanones

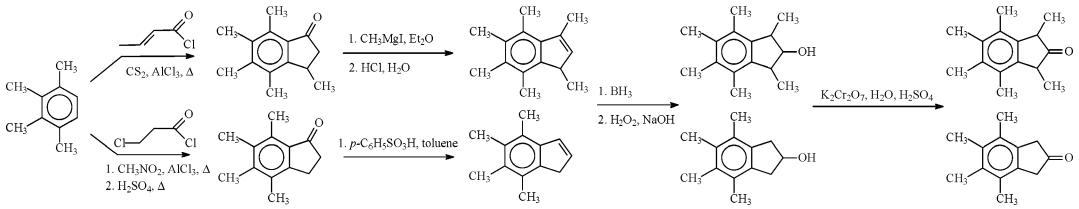

Scheme 3. Synthesis of 2 via Negishi Reaction

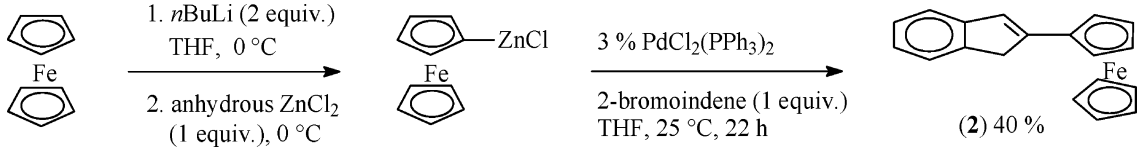

systems.[25] To this purpose, we have prepared a series of (ferrocenyl)indenes, that is, (2-ferrocenyl)indene, (2-ferrocenyl)-tetramethylindene, (2-ferrocenyl)hexamethylindene, (3-ferrocenyl)indene, and (3-ferrocenyl)hexamethylindene. Here we describe the synthesis and the structural and spectroscopic characterization of the neutral precursors as well as the optical properties of the derived ferrocenium cations in the UV−vis and near-IR regions. The accurate analysis of the frontier orbitals and the calculation of the main electronic absorptions allow assessing the role of the geometric and electronic factors in the modulation of the energy and intensity of aryl-ferrocenium charge transfer bands.

Results and Discussion

Synthesis. The isomeric (3-ferrocenyl)indene (**1**) and (2-ferrocenyl)indene (**2**) were prepared by Plenio[26a] (Scheme 1) starting from the commercial 2-indanone and 3-indanone and ferrocenyl lithium. Whereas the 3-isomer was produced in satisfactory yield (40%), the low yield of 2-isomer (12%) is due to the preferential formation of the enolate.

The synthesis of the methylated **3**−**5** required the preparation of the corresponding indanones. The procedure adopted for the preparation of the methylated 2-indanones is described in Scheme 2. Alternatively, a higher yield of **2** (40%) along with 1,1′-bis(2-indenyl)ferrocene (47%) could be obtained with the Negishi reaction consisting in the Pd(0)-catalyzed cross-coupling between 1,1′-zincated ferrocene and (2-bromo)indene.[26c] Lately, we have optimized the synthesis of **2** under milder conditions by using a modified procedure of the above-mentioned Pd-catalyzed reaction, obtaining complex **2** selectively and in good yield (40%) and only trace amount of 1,1′-bis(2-indenyl)-ferrocene (Scheme 3).

The critical step was the conversion of the methylated indenes to the corresponding 2-indanones. In fact, the commonly used methods via epoxidation with *m*-chlorobenzoic acid in biphasic CH_2Cl_2/H_2O (pH = 8) medium or with *N*-bromosuccinimide in THF/water, followed by ketone formation catalyzed by Lewis acids, were unsuccessful. The desired 2-indanones were obtained by hydroboration of 4,5,6,7-tetramethylindene and 1,3,4,5,6,7-hexamethylindene with BH_3 followed by oxidation with H_2O_2/NaOH. The resulting 2-indanol derivatives (80%) were easily converted to tetra- and hexamethylindanone by oxidation with a chromic mixture. The synthesis of the hexamethylindan-1-one was previously reported.[27] Finally, addition of ferrocenyllithium followed by hydrolysis and elimination of water yielded (3-ferrocenyl)hexamethylindene (**3**), (2-ferrocenyl)tetramethylindene (**4**) (20%), and (2-ferrocenyl)hexamethylindene (**5**) (35%) (Scheme 1).

Molecular Structures. We have previously reported[28] the molecular structures of (3-ferrocenyl)indene (**1**) and (2-ferrocenyl)indene (**2**) (Figure 1a). In complex **1** the Cp-indene ligand assumes a nonplanar geometry with the benzene ring oriented toward iron in order to avoid repulsive interactions between the hydrogen atoms H1 and H3 of the cyclopentadienyl ring and H12 and H16 of the benzene ring.

The observed molecular structure is achieved by a rotation of 25−26° (Table 1) of the indene plane about C2−C11. On the contrary, in complex **2** the Cp-indene ligand is almost planar, as imposed by an operative π-electron resonance and in part by the requirement to make the Cp ring (C1 throughout C5) bisect the angle H12−C12−H12′ such as to minimize the contact interactions between H1 and H12, H12′. With respect to the calculated conformation (Table 1) the torsion angle about C2−C11 is appreciably different. We note that the observed X-ray structure of **2** is also influenced by crystal field forces, which lead to the reported structural differences mainly regarding the torsion angle about C2−C11. An inspection of the mode of packing of **2** (Figure 1b) shows a clear organization of molecules in which the planes of the Cp rings of the ferrocenyl groups approach the six-membered ring of the indene group at short van der Waals distances in the range 3.6−3.8 Å. This feature might induce a parallelism of these planes and as a consequence a torsion angle about C2−C11 very close to 0°.

In the molecular structure obtained for (2-ferroceny)hexamethylindene (**5**) (Figure 1a, Table 2) the indene group and the σ-bonded Cp ring of the ferrocene moiety are far away from coplanarity in order to optimize and balance the nonbonded interactions between H1−H12 (2.42 Å) and H1−C20 (3.27 Å). The torsion angle C1−C2-C11−C12 here is ca. 25−26°, a value almost identical to that found for complex **1**. Any rotation about the bond C2−C11 is strongly prevented; thus the resulting

(25) (a) Creutz, C.; Newton, M. D.; Sutin, N. *J. Photochem. Photobiol. A: Chem.* **1994**, *82*, 47−59. (b) Evans, C. E. B.; Ducharme, D.; Naklicki, M. L.; Crutchley, R. J. *Inorg. Chem.* **1995**, *34*, 1350−1354. (c) Desjardins, P.; Yap, G. P. A.; Crutchley, R. J. *Inorg. Chem.* **1999**, *38*, 5901−5905.

(26) (a) Plenio, H. *Organometallics* **1992**, *11*, 1856−1859. (b) Lee, S. G.; Lee, S. S.; Chung, Y. K. *Inorg. Chim. Acta* **1999**, *286*, 215−220. (c) Anderson, J. C.; White, C.; Stenson, K. P. *Synlett* **2002**, *9*, 1511−1513.

(27) (a) Westcott, S. A.; Kakkar, A. K.; Stringer, G.; Taylor, N. J.; Marder, T. B. *J. Organomet. Chem.* **1990**, *394*, 777−794. (b) O'Hare, D.; Green, J. C.; Marder, T.; Collins, S.; Stringer, G.; Kakkar, A. K.; Kaltsoyannis, N.; Kuhn, A.; Lewis, R.; Mehnert, C.; Scott, P.; Kurmoo, M.; Pugh, S. *Organometallics* **1992**, *11*, 48−55. (c) O'Hare, D.; Murphy, V. J.; Kaltsoyannis, N. *J. Chem. Soc., Dalton Trans.* **1993**, 383−392.

(28) Santi, S.; Ceccon, A.; Crociani, L.; Gambaro, A.; Ganis, P.; Tiso, M.; Venzo, A.; Bacchi, A. *Organometallics* **2002**, *21*, 565−574.

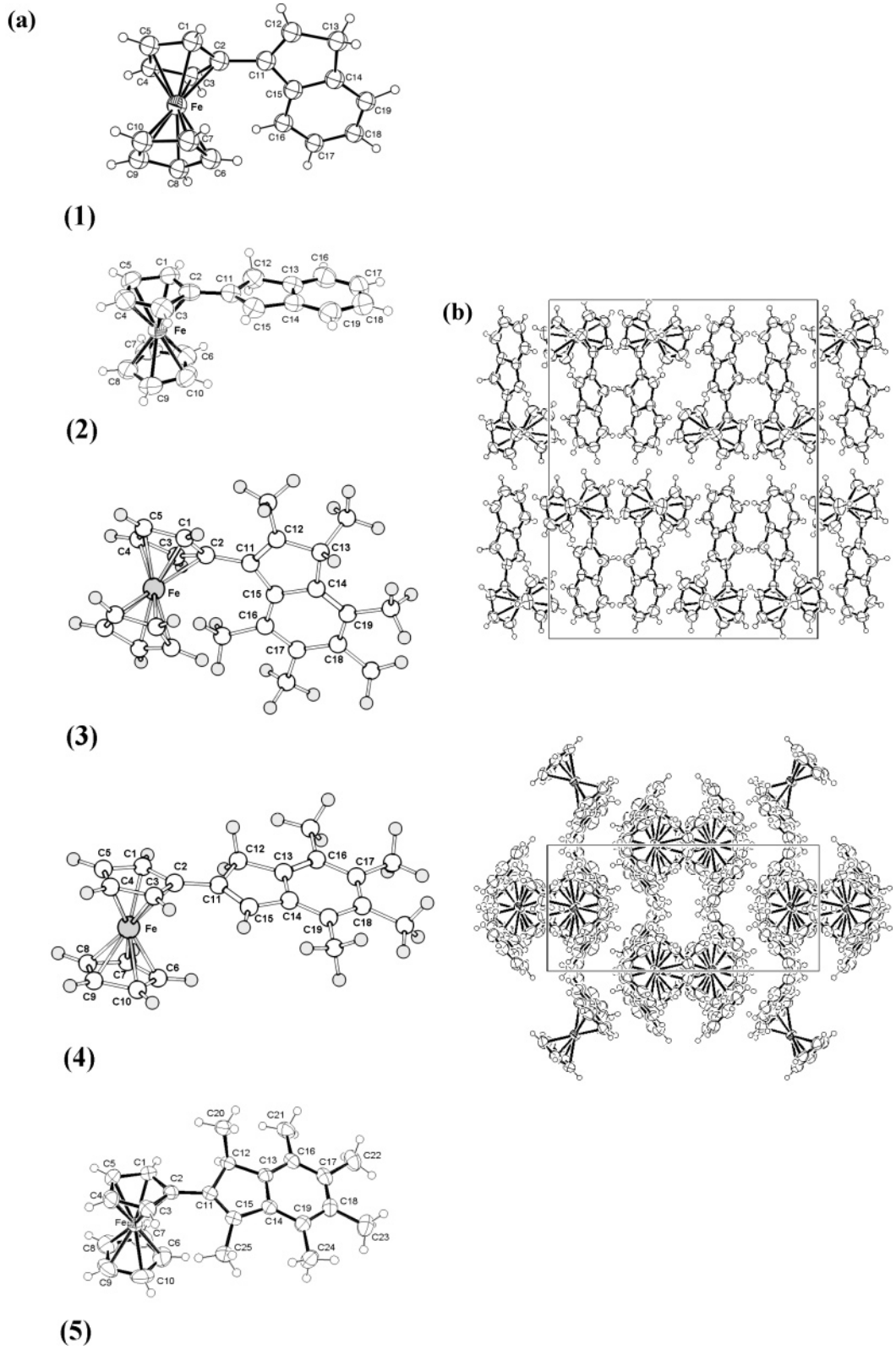

Figure 1. (a) Molecular structures of **1** (X-ray), **2** (X-ray), **3** (DFT-optimized geometry), **4** (DFT-optimized geometry), and **5** (X-ray). Hydrogen atoms are not labeled for clarity. (b) Mode of packing of complex **2** as viewed along b (top) and a (bottom).

molecule may be regarded as a *prochiral* center giving rise to two distinct *atropoisomers*.[29] Due to the presence of the stereoisomeric center on C12, two stereoisomers are predictable for each of the two *atropoisomeric* configurations, though the *transoid* orientation of the ferrocenyl group with respect to the methyl group C20 seems to be preferred for steric reasons (Figure 1a). The resulting nonplanar conformation of **5** might hamper significant π-electron resonance in the overall molecular system. Besides this feature, all the geometrical parameters are quite in the norm.

(29) Complexation on either of the two faces of the indene moiety is not equivalent and would produce two distinct configurations and their corresponding atropoisomers. (a) Hall, D. M. *Progr. Stereochem.* **1969**, *4*, 1−42. (b) Öki, M. *Top. Stereochem.* **1983**, *14*, 1−81.

Table 1. Selected Intratomic Distances (Å) and Angles (deg) (crystallographic data are indicated in italics with their standard deviation)

	1	**1**$^+$	**2**	**2**$^+$	**3**	**3**$^+$	**4**	**4**$^+$	**5**	**5**$^+$
Fe−Q1[a]	1.66	1.72	1.67	1.71	1.67	1.71	1.66	1.70	1.66	1.70
	1.638(3)		*1.655(5)*						*1.653(4)*	
Fe−Q2[a]	1.67	1.73	1.66	1.72	1.67	1.72	1.67	1.71	1.67	1.71
	1.63(4)		*1.648(5)*						*1.652(4)*	
Q1−Fe−Q2	179	179	179	177	176	176	179	176	179	176
	179.1(3)		*179.0(3)*						*178.7(3)*	
D1(C1−C2−C11−C12)[b]	−25	−29	15	14	−32	−33	16	16	25	24
	−23.0(4)		*−2.0(6)*						*26.0(4)*	
D2(C3−C2−C11−C15)[b]	−27	−22	13	5	−39	−32	15	8	27	18
	−25.8(5)		*−5.7(7)*						*27.1(5)*	
D3(C1−C2−C11−C15)[b]	152	154	−168	−168	139	144	−166	−165	−153	−160
	153.8(3)		*−176.1(4)*						*−155.0(3)*	
D4(C3−C2−C11−C12)[b]	156	155	−164	−173	151	151	−164	−171	−156	−157
	157.5(3)		*−176.1(4)*						*−151.9(3)*	
γ[c]	26.4	25.93.	15.6	13.4	31.2	31.7	16.7	14.9	21.6	23.6
	24.5(2)		*3.9(2)*						*23.7(1)*	

[a] Q1 and Q2 indicate the centroids of the Cp ring bonded to indene and of the free Cp ring respectively. [b] D1, D2, D3, and D4 are dihedral angles. [c] Angle between the planes containing rings C1−C2−C3−C4−C5 and C11−C12−C13−C14−C15.

Table 2. Crystallographic Structure of 5

formula	$C_{25}H_{28}Fe$
fw	384.32
cryst syst	triclinic
space group	$P\bar{1}$
a/Å	11.264(3)
b/Å	11.734(3)
c/Å	9.066(2)
α/deg	94.56(3)
β/deg	108.39(3)
γ/deg	117.58(3)
V/A^3	970.9(4)
Z	2
D_{calc}/g cm^{-3}	1.315
F(000)	408
μ(Mo Kα)/mm^{-1}	0.782
λ(Å)	0.71073
T	293(2)
no. of reflns collected	4837
no. of reflns obsd [$I \geq 2\sigma(I)$]	4311
final R1, wR2[a]	0.045, 0.105

[a] $R1 = \sum||F_o| - |F_c||/\sum|F_o|$; $wR2 = [\sum[w(F_o^2 - F_c^2)^2]/\sum w(F_o^2)^2]]^{1/2}$.

Electrochemistry. Cyclic voltammograms (CVs) of complexes **1**−**5** were recorded under argon in CH_2Cl_2/0.1 M *n*-Bu_4NPF_6. All the complexes show two oxidation waves in the range from 0 to 2 V vs SCE (Figure 2, Table 3).

The first oxidation wave is chemically and electrochemically reversible as expected for a Fc/Fc$^+$ redox couple, and it occurs at a potential that decreases with methylation of the indene group in the range 0.42−0.51 V. The second wave is assigned to indene oxidation and is chemically irreversible, but E_p reaches a constant value by increasing the scan rate. Its chemical reversibility is evident in the methylated complexes and its oxidation potential strongly decreases from 1.8 to 1.3 V depending on methylation and on varying the position of ferrocene from C3 to C2 double-bond carbon atoms. The coplanarity and the consequent π-conjugation of the Cp-indene are determined by the position of the ferrocenyl group and by the methyl substituents, being almost realized when the ferrocene is in 2-position and the methyls are absent in the Cp moiety of indene. Both π-conjugation of Cp-indene carbon atoms and the presence of electron-donating substituents make the oxidation of the indene group easier. In several materials containing a π-conjugated organic molecule linked to transition metal units redox-matching of the metal and organic components is a requisite for the enhancement of their conductivity.[1,19c,d]

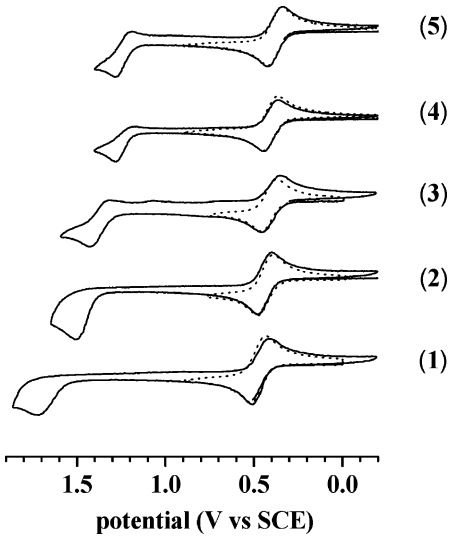

Figure 2. Cyclic voltammetry of complexes **1**−**5** in CH_2Cl_2/0.1 M *n*-Bu_4NPF_6 at scan rate $v = 0.5$ V s^{-1} except **3**, at $v = 5$ V s^{-1}.

Table 3. Cyclic Voltammetric Data[a]

complex	E_p^1	$E_{pa}^1 - E_{pc}^1$	E_p^2	$E_{pa}^2 - E_{pc}^2$	ΔE[b]
1	0.51[c]	0.086[c]	1.85[c]		1.34[c]
2	0.46[d]	0.078[d]	1.54[d]		1.08_5[d]
3	0.46[e]	0.085[e]	1.43[e]	0.107[e]	0.97_5[e]
4	0.44	0.077	1.28	0.100	0.84
5	0.42	0.078	1.28	0.091	0.86

[a] Solvent CH_2Cl_2/0.15 M *n*-Bu_4NBF_4; potential volts vs SCE at a 0.5 mm diameter gold disk electrode, $T = 20$ °C; potential scan rate 0.5 V s^{-1}. [b] $\Delta E = E_p^2 - E_p^1$. [c] At 50 V s^{-1}. [d] At 10 V s^{-1}. [e] At 5 V s^{-1}.

Optical Spectroscopy. The UV−vis electronic spectra of the neutral complexes **1**−**5** between 270 and 800 nm are reported in Figure 3.

All the compounds display two weak bands at ca. 340 and 450 nm, which are commonly assigned to the metal-centered d−d transitions of the ferrocenyl group.[5c,15c,30] In addition, the spectra of the 2-isomers **2**, **4**, and **5** display a more intense absorption band at 312, 320, and 318 nm, respectively, usually attributed to the $\pi-\pi^*$ transitions of the aryl group bonded to the ferrocene.[30] Interestingly, for the 3-isomers **1** and **3** this band is much less intense and blue-shifted at 286 and 300 nm,

(30) Sohn, Y. S.; Hendrikson, D. N.; Gray, H. B. *J. Am. Chem.* Soc. **1971**, *93*, 3603−3612.

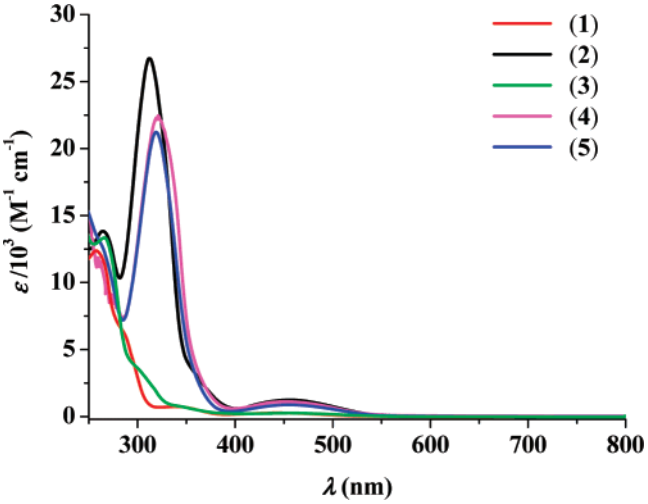

Figure 3. UV−vis spectra of **1**−**5** in CH_2Cl_2.

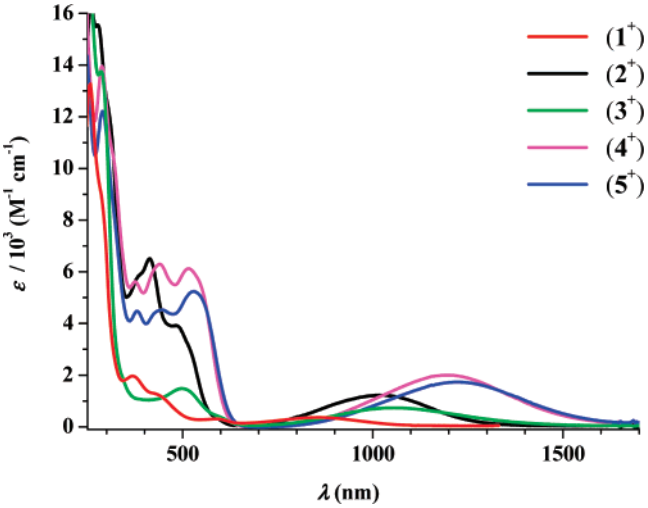

Figure 4. UV−vis−near-IR of $\mathbf{1}^+$−$\mathbf{5}^+$ in CH_2Cl_2.

respectively. This shift is due to the less efficient donor capability of the ferrocenyl substituent in the 3-position than in the 2-position.

The spectra of the cations $\mathbf{1}^+$−$\mathbf{5}^+$ (Figure 4) obtained by stepwise oxidation in the range 0.0−0.6 V of the neutral compounds in an OTTLE spectroelectrochemical cell at room temperature display almost complete reversibility (≥95%) upon cathodic scan reversal except for $\mathbf{3}^+$, which partially decomposes. The band at highest energy undergoes a significant blue-shift (ca. 32 nm) due to the ferrocenium group acting as an electron-withdrawing group. The bands in the visible region are replaced by a structured band grouping covering a wide range from 350 to 650 nm, whose structure and intensity depend on the position of the ferrocenium group and on the methylation.

However, the most significant spectral change occurs in the near-IR region of the spectrum, where a new broad, low-energy absorption band appears in the range between 840 and 1220 nm (Table 4). Similar bands have been observed in other conjugated ferrocenyl aryl complexes and have been assigned to aryl to iron ligand-to-metal charge transfer (LMCT) transitions.[15,19c,d] Also the energy of these bands depends on the position of the ferrocenyl group with respect to the indene and on the degree of methylation. Moreover, the energy of the LMCT bands correlates with the oxidation potential difference ΔE between the indene (donor) and the ferrocenium (acceptor) (Figure 5).

Table 4. Near-IR Data[a]

cation	$\tilde{\nu}_{max}$ [b] [cm^{-1}]	ϵ_{max} [mol^{-1} dm^3 cm^{-1}]	$f \times 10^3$ [c] [cm^{-1}]
$\mathbf{1}^+$	11620	360	5.54
$\mathbf{2}^+$	9830	1223	15.36
$\mathbf{3}^+$	9480	734	14.46[d]
$\mathbf{4}^+$	8200	1998	28.00
$\mathbf{5}^+$	8370	1729	23.90

[a] Solvent was CH_2Cl_2/*n*-Bu_4NPF_6, T = 20 °C. [b] ± 4 cm^{-1}. [c] Oscillator strength of LMCT band calculated from the sum of fitted *n* Gaussians, $f = (4.6 \times 10^{-9})\sum_n(\epsilon_{max}\Delta\tilde{\nu}_{1/2n})$. See ref 25b. [d] $\mathbf{3}^+$ decomposes during the acquisition of the spectrum.

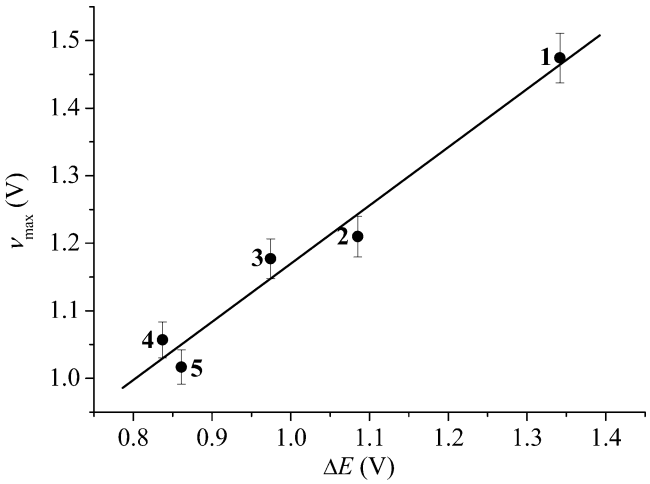

Figure 5. Optical energy (ν_{max}) of the near-IR transition vs oxidation potential difference (ΔE) for $\mathbf{1}^+$−$\mathbf{5}^+$.

The electrochemical and spectroscopic results can be interpreted by using the classical two-state electron transfer model (Hush theory) applied to LMCT and MLCT transitions.[25] The optical energy $E_{op} = \nu_{max}$ of a LMCT band is related to the electrochemical potential difference ΔE by eq 1:[20]

$$\nu_{max} = \Delta E + \Delta E' + \lambda \quad (1)$$

Here, $\Delta E'$ represents the difference between the $Fe^{II/III}$ oxidation potential with the oxidized indene and the measured $Fe^{II/III}$ potential, and λ the reorganizational energy. Provided that $\Delta E'$ and λ are constant, a plot of ν_{max} versus ΔE is linear and this occurs for the $\mathbf{1}^+$−$\mathbf{5}^+$ series, the only variable being the position and the structure of the indene. The least-square fit of the data (Figure 5) gave a slope of 0.86 ± 0.09 with R = 0.98, in quite good agreement with the theoretical value of the unit. This correlation indicates that the smaller the oxidation potential difference between the donor and acceptor, the lower the energy of the optical transition.

The molar absorption coefficient (ϵ_{max}) of the LMCT (Table 4) bands in the oxidized complexes $\mathbf{1}^+$−$\mathbf{5}^+$ increases by decreasing the ΔE (Table 3). For a Gaussian-shaped peak the oscillator strength (f) is related to ϵ_{max} and can be experimentally determined by using eq 2, where $\Delta\tilde{\nu}_{1/2}$ represents the half-bandwidth:[20,21]

$$f = (4.6 \times 10^{-9})\epsilon_{max}\Delta\tilde{\nu}_{1/2} \quad (2)$$

A linear correlation (R = 0.995) of f as a function of ΔE within the series of the ferrocenyl cations $\mathbf{1}^+$−$\mathbf{5}^+$ (Figure 6) is found, except $\mathbf{3}^+$, which decomposes during the acquisition of the spectrum.

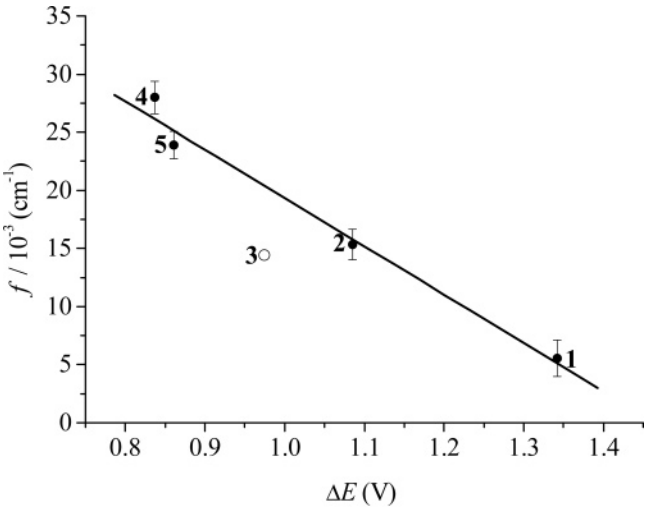

Figure 6. Oscillator strength (f) of near-IR transition vs oxidation potential difference (ΔE) for $\mathbf{1}^+-\mathbf{5}^+$.

This behavior clearly indicates that the smaller the potential difference between donor and acceptor, the greater the oscillator strength in the charge transfer transition. Hush demonstrated that the intensity of a charge transfer transition is related to the extent of coupling between donor and acceptor. The derivation begins by considering the theoretical expression for f (eq 3), where G is the degeneracy of the states concerned and D is the dipole strength of the electric dipole transition, which is related to the charge transfer transition dipole moment (M) (eq 4) and the elementary charge (e):

$$f = (1.85 \times 10^{11}) G \tilde{\nu}_{max} D \quad (3)$$

$$M = eD^{1/2} \approx \alpha eR \quad (4)$$

In turn, M is related to the length of the transition dipole R and to the delocalization coefficient α, which is a measure of the charge delocalization. Reasonably assuming that R does not vary significantly within the series $\mathbf{1}^+-\mathbf{5}^+$, larger dipole moments correspond to greater charge delocalization. On the basis of the linear correlation of both $\tilde{\nu}_{max}$ and f with ΔE found for the series of cationic complexes studied, it is clear that also M correlates with ΔE. Smaller differences in donor and acceptor oxidation potentials correspond to larger charge transfer transition dipole moments and more efficient charge transfer. Similar correlations have been previously observed for other LMCT transitions in Fc-conjugated cations.[15a,c,19c] The highest f value is found for the tetramethylated 2-isomer $\mathbf{4}^+$, in which the absence of methyl groups in the 1,3 position assures the almost planarity of the Cp-indene ligand. In fact, the introduction of the two additional methyls in $\mathbf{5}^+$ imposes a rotation of ca. 26° around the C2−C11 σ-bond linking the Cp and the indene moieties. Moreover, in spite of its distorted structure characterized by a Cp-indene dihedral angle of 32−33°, a significant value of f (underestimated because of its decomposition) is retained in the hexamethylated 3-isomer $\mathbf{3}^+$, higher than in the unsubstituted $\mathbf{1}^+$ and at least similar to $\mathbf{2}^+$. We can conclude that along the series $\mathbf{1}^+-\mathbf{5}^+$ it is the methylation of the indene that mainly rules the extent of the charge transfer transition dipole moment M and, consequently, the efficiency of indene-to-iron charge transfer. Similar considerations can be made for the red-shift of the band energy, the values of $\tilde{\nu}_{max}$ decreasing in the order $\mathbf{1}^+ > \mathbf{2}^+ > \mathbf{3}^+ > \mathbf{4}^+ \approx \mathbf{5}^+$.

DFT Analysis. The present computational analysis aims mainly at determining the structures of both the neutral and the monooxidized iron complexes and at calculating their electronic spectra for a correct assignment of the UV−vis−near-IR absorptions and for a plausible explanation of the observed energy shifts when replacing four or six H atoms of the indene moiety with methyl groups.

The neutral complexes **1**, **2**, and **5** were optimized without any constraint (see Computational Details) starting from the crystallographic structures of 3-ferrocenylindene,[28] 2-ferrocenylindene,[13] and hexamethyl-2-ferrocenylindene (Figure 1a), respectively. For the full geometry optimization of **3** the initial structure was obtained by replacing six H atoms of the indene ring of **1** with methyl groups. Finally, the starting geometry of **4** was generated by replacing the methyl groups of **5** bonded to C12 and C15 with H atoms. A very good agreement is found between the calculated molecular geometries and the corresponding available crystallographic structures (Table 1). The strongest deviation is observed for the dihedral angle of **2** about the C2−C11 σ-bond, which is larger in the computed geometry likely due to the absence of the previously discussed crystal-packing effect in the modeling. No significant differences are observed in the interatomic distances and angles of the ferrocenyl pendants of **1**−**5**. Instead, the average indene C−C bond length slightly increases with the number of methyl susbstituents (≈0.015 Å), but bond alternation is maintained. As previously reported,[12,13] in **2** the Cp and the indene moieties are almost coplanar; on the contrary in **1** the Cp ring is tilted from the indene plane by approximately 26°. Complex **4** is structurally very similar to **2**, while in **5** a significant dihedral angle about the C2−C11 σ-bond linking the Cp and the indene moieties is measured (≈26°). Interestingly, the value of this dihedral angle is the same as measured in **1**, but of opposite sign (Table 1 and Figure 1a). For complex **3** structural features analogous to those of **1** are calculated, with appreciable increase of the dihedral angle about the C2−C11 σ-bond (≈35°), resulting from the steric hindrance of the methyl groups.

The HOMOs of **2**, **4**, and **5** have a strongly weighted contribution on the iron center, decreasing when increasing the number of methyl substituents on the indene moiety (Table 5).[31] In the HOMOs of **1** and **3** the percentage of iron is higher and essentially constant (Table 5). An analogous albeit opposite trend is found for the indene percentage contribution to the HOMOs, which increases when going from 3-isomers, **1** and **3**, to 2-isomers, **2**, **4**, and **5**, and increases in these last ones with increasing the number of methyl substituents. The LUMOs of **1**, **2**, and **4** are mainly indene-based molecular orbitals, although important contributions localized on the ferrocenyl unit are present (Table 5). Notably, in the hexamethylated complexes the percentage of iron in the LUMO becomes comparable (complex **5**) and even higher (complex **3**) than the percentage of indene. On the basis of the HOMO−LUMO gap, the electronic effect of the methylation is an enhanced stability of the neutral species.

Upon oxidation, the relevant structural changes involve the distances between the iron atom and the centroids of its coordinated Cp rings, which increase by ∼0.05 Å in all cases (Table 1).

In $\mathbf{1}^+$, $\mathbf{2}^+$, and $\mathbf{3}^+$ the highest occupied β-spin orbital is the highest occupied level (Hβ), while in $\mathbf{4}^+$ and $\mathbf{5}^+$ the highest occupied level is an α-spin orbital (Hα), which has qualitatively the same topology of the HOMOs of the neutral precursors. All the charged compounds are polarized; the spin density is

(31) Pictures of the frontier Kohn−Sham MOs of complexes $\mathbf{1}^{0/+1}-\mathbf{5}^{0/+1}$ calculated at ZORA/TZP small frozen core are included in the Supporting Information.

Table 5. Significant Electronic Parameters (ZORA, TZP small frozen core level of theory) (energies of the Kohn−Sham MOs are in eV)

	1	**1**$^+$	**2**	**2**$^+$	**3**	**3**$^+$	**4**	**4**$^+$	**5**	**5**$^+$
Fe[a]	−0.067	0.034	−0.065	0.019	−0.070	−0.001	−0.066	0.003	−0.068	−0.002
spin density[b]		1.01		0.89		0.74		0.75		0.72
IP (eV)[c]	6.47		6.29		6.14		6.01		5.95	
H-L	2.405		2.190		2.480		2.232		2.294	
H	−4.121		−4.147		−3.986		−3.993		−3.959	
L	−1.716		−1.957		−1.506		−1.761		−1.665	
H%Fe[d]	78.1		74.0		79.4		68.4		66.5	
H%Cp_2[d]	10.5		7.2		11.0		6.1		8.6	
H%Ind[d]	2.2		3.4		2.1		8.5		12.5	
L%Fe[e]	21.3		25.4		38.8		28.7		32.8	
L%Cp_2[e]	6.6		12.7		22.6		14.1		15.7	
L%Ind[e]	34.6		48.7		24.0		42.0		35.8	
Hα-Lα		2.097		2.117		2.158		2.065		2.097
Hβ-Lβ		0.371		0.588		0.268		0.571		0.567
Hα		−8.724		−8.591		−8.055		−8.068		−7.956
Lα		−6.627		−6.474		−5.897		−6.003		−5.859
Hβ		−8.660		−8.551		−7.938		−8.100		−8.000
Lβ		−8.289		−7.963		−7.670		−7.529		−7.433

[a] Voronoi atomic charges. [b] Mulliken spin densities. [c] Adiabatic ionization potentials. [d] Percentage contributions of the Cp rings (Cp_2), iron (Fe), and indene (Ind) to the Kohn−Sham highest occupied molecular orbital (H). [e] Percentage contributions of the Cp rings (Cp_2), iron (Fe), and indene (Ind) to the Kohn−Sham lowest occupied molecular orbital (L).

prominently localized on iron, decreasing in the order **1**$^+$ > **2**$^+$ > **4**$^+$ ≈ **3**$^+$ ≈ **5**$^+$, i.e., the same sequence established for the computed Voronoi charge of the iron nucleus (Table 5) that nicely compares to the trend of the extent of intramolecular charge transfer detected with the spectroelectrochemical measurements. As reported in Table 5, the gap between the highest occupied spin orbital and the corresponding lowest empty level is much larger in the methylated than in the nonmethylated ions.

The calculated adiabatic ionization potentials in vacuo well match the trend of the $E_{1/2}$ of the voltammetric first wave (Table 3). The value of the couple **1**/**1**$^+$ is higher than the value computed for the couple **2**/**2**$^+$, i.e., 6.47 versus 6.29 eV. In addition the presence of the methyl groups lowers the adiabatic ionization potentials, which are 6.14 eV (**3**/**3**$^+$), 6.01 eV (**4**/**4**$^+$), and 5.95 eV (**5**/**5**$^+$). Two important observations can be drawn: (i) the greater the extent of planarity of the Cp-indene moiety, the easier the oxidation of the complex, as revealed by comparing the couples **1**/**1**$^+$ and **2**/**2**$^+$ and the couples **3**/**3**$^+$ and **5**/**5**$^+$, and (ii) the electronic effect of the methyl groups bonded to the indene is a net lowering of the oxidation potential of the iron nucleus. The availability of the three couples **3**/**3**$^+$, **4**/**4**$^+$, and **5**/**5**$^+$ clearly allows a fine detection of the interplay between the planarity of the Cp-indene and the extent of methylation (Table 5).

PCM-TD-DFT calculations were carried out on the optimized geometries of the neutral and charged complexes to investigate in detail their electronic spectra at the B3LYP/LANL2DZ,6-31+G* level of theory (see Computational Details). The lowest 15 excitation energies were computed covering approximately the range 3000−400 nm. The salient spectral features are well reproduced by PCM-TD-DFT calculations, especially those of the neutral complexes (Table 6).

No absorptions in the near-IR region are predicted for **1**−**5**, in agreement with the experimental results. The lowest computed absorption for each neutral complex occurs in the visible region in the range 455−475 nm and, as experimentally observed (range 443−454 nm), does not significantly change when increasing the number of methyls bonded to indene, i.e., from **1** to **3** and from **2** to **4** and to **5** (Table 6). For the 3-isomers this band occurs at slightly higher energy, i.e., much nearer to the band experimentally detected for ferrocene in the same conditions at 435 nm, which is commonly assigned to iron d−d transitions.[30] For the ferrocene derivatives **1**−**5** this band in the visible region maintains d−d character, but is in part due also to Fe-to-indene charge transfer, that is, to a metal-to-ligand charge transfer (MLCT) process, which results in a more important contribution in 2-isomers rather than in 3-isomers (Table 6).[32] In the second relevant and much more intense electronic absorption of the neutral complexes **1**−**5**, which occurs in the experimental spectrum between 313 and 332 nm, and is computed in the range 301−334 nm, the HOMO−LUMO transition is dominating over the other contributions (Table 6). Since the HOMO−LUMO gap is larger in the 3-isomers than in the 2-isomers, in the spectra of **1** and **3** this band is slightly blue-shifted.

The lowest PCM-TD-DFT computed absorption of the radical cations **1**$^+$−**5**$^+$ occurs in the near-IR region, in agreement with the experiments (Table 7).

The excitation energies nicely match the trend of the maxima obtained by deconvolution of the electronic spectra: 707 nm (**1**$^+$, expt 860 nm) < 848 nm (**2**$^+$, expt 1017 nm) < 946 nm (**3**$^+$, expt 1055 nm) < 992 nm (**4**$^+$, expt 1220 nm) ≈ 1017 nm (**5**$^+$, expt 1195 nm), within the range of error typically reported in similar large, open-shell complexes. These absorptions have mainly Hβ-Lβ and Hα-Lα contributions, and on the basis of the topology of these couples of spin molecular orbitals they can be assigned to ligand-to-metal charge transfer processes (LMCT), i.e., from the indene moiety to iron (Figure 7). Interestingly, a minor contribution of increasing importance going from **1**$^+$ to **5**$^+$ comes from a monoelectronic transition between (H-3)β, which is iron centered, to Lβ, which is in part indene centered; this can be associated with the reverse MLCT process. Finally, several absorptions have been calculated for **1**$^+$−**5**$^+$ in the range 300−550 nm, but the numerous contributions from different monoelectronic transitions precluded a precise assignment. Anyway, the computed excitation energy values are in rather good agreement with the experimental peaks obtained by deconvolution: 450 nm (osc. strength 0.001) for **1**$^+$ (expt 454 nm), 440 nm (osc. strength 0.11) and 413 nm (osc. strength 0.006) for **2**$^+$ (expt 480 and 410 nm), 484 nm (osc. strength 0.002) for **3**$^+$ (expt 498 nm), 540 nm (osc. strength 0.008) and 460 nm (osc. strength 0.15) for **4**$^+$ (expt 535 and

(32) Pictures of selected Kohn−Sham MOs of complexes **1**$^{0/+1}$−**5**$^{0/+1}$ calculated at PCM-B3LYP/LANL2DZ,6-31+G* are included in the Supporting Information.

Table 6. Computed Excitation Energies (PCM-B3LYP/LANL2DZ, 6-31+G* level of theory) and Experimental Spectral Data of the Neutral Complexes 1−5

	PCM-TD-DFT[a]	electronic	transitions[b]	assign.	exptl values[c]
	4.00 eV (0.027)	73 → 77	0.25154		
	310 nm	73 → 74	0.54265	H−L, MLCT	332 nm(w)
		70 → 74	−0.21102		
1		70 → 75	0.26765		
	2.66 eV (0.0009)	70 → 77	0.33302	d−d, MLCT	448 nm(w)
	465 nm	72 → 76	0.36400		
		73 → 74	0.12935		
	3.79 eV (0.63)	71 → 74	−0.21025		
	327 nm	73 → 74	0.53150	H−L	313 nm(i)
		70 → 74	0.29970		
2	2.61 eV (0.004)	70 → 77	0.35764		
	475 nm	72 → 76	0.37414	MLCT, d−d	454 nm(w)
		73 → 74	0.14202		
	4.12 eV (0.128)	97 → 101	0.15363		
	301 nm	97 → 98	0.58916	H−L	327 nm
		96 → 99	0.30156		
3	2.67 eV (0.0014)	95 → 100	−0.26190		
	465 nm	93 → 99	−0.29054	d−d	447 nm (w)
		93 → 100	0.24852		
	3.71 eV (0.71)	87 → 90	−0.24056		
	334 nm	89 → 90	0.56319	H−L, MLCT	322 nm (i)
		85 → 90	−0.30530		
4	2.61 eV (0.0054)	85 → 92	0.35524		
	475 nm	88 → 91	0.39245	MLCT, d−d	443 nm (w)
		89 → 90	0.13257		
	3.78 eV (0.62)	95 → 98	−0.25859		
	328 nm	97 → 98	0.56441	H−L, MLCT	318 nm (i)
		93 → 98	−0.31174		
5	2.61 eV (0.004)	93 → 100	0.30975		
	474 nm	96 → 99	0.33472	MLCT, d−d	447 nm (w)
		97 → 98	0.12828		

[a] Excitation energy (in eV and nm) and computed oscillator strength in parentheses. [b] The main monoelectronic transitions are reported with the corresponding CI coefficient. The HOMO and the LUMO are 73,74 (**1**), 73,74 (**2**), 97,98 (**3**), 89,90 (**4**), and 97,98 (**5**). [c] Values obtained by deconvolution of the electronic spectra with Gaussian functions; the maxima are labeled i (intense) and w (weak).

Table 7. Computed Excitation Energies in the Near-IR Region (PCM-B3LYP/LANL2DZ,6-31+G* level of theory) and Experimental Spectral Data of the Monooxidized Complexes 1^+−5^+

	PCM-TD-DFT[a]	electronic transitions[b]	assign.	exptl values[c]
$\mathbf{1}^+$	1.75 eV (0.01)	73α → 74α 0.30145	LMCT	860 nm (w)
	707 nm	72β → 73β 0.92817		
$\mathbf{2}^+$	1.46 eV (0.027)	73α → 74α 0.49341	LMCT	1017 nm (w)
	848 nm	69β → 73β −0.10037		
		72β → 73β 0.88659		
$\mathbf{3}^+$	1.31 eV (0.014)	97α → 98α −0.25041	LMCT	1055 nm (w)
	946 nm	93β → 97β 0.16310		
		96β → 97β 0.95050		
$\mathbf{4}^+$	1.25 eV (0.041)	89α → 90α 0.46075	LMCT	1220 nm (w)
	992 nm	85β → 89β −0.32540		
		88β → 89β 0.86112		
$\mathbf{5}^+$	1.22 eV (0.043)	97α → 98α −0.42172	LMCT	1195 nm (w)
	1017 nm	93β → 97β 0.42875		
		96β → 97β 0.87184		

[a] Excitation energy (in eV and nm) and computed oscillator strength in parentheses. [b] The main monoelectronic transitions are reported with the corresponding CI coefficient. [c] Values obtained by deconvolution of the electronic spectra with Gaussian functions; the maxima are labeled i (intense) and w (weak).

431 nm), and 551 nm (osc. strength 0.001) and 460 nm (osc. strength 0.15) for $\mathbf{5}^+$ (expt 551 and 440 nm).

Conclusions

The electrochemical and optical results obtained for the series of complexes **1**−**5** and of the corresponding monooxidized cations $\mathbf{1}^+$−$\mathbf{5}^+$ have shown that the modulation of the donor−acceptor interaction is feasible and proceeds from the interplay of several factors, that is, the position of the ferrocene/ferrocenium with respect to the indene, the planarity of the Cp-indene ligand, and the degree of methylation. In the neutral compounds the dominant factor is the position of the ferrocene group. In fact, the UV−vis spectra of the 2-isomers display two characteristic, very intense, and low-energy bands due to a more extensive conjugation between ferrocene and indene. Conversely, the substituent effect of the methyl groups for the cationic complexes is much stronger than for the neutral derivatives. Here, the electronic interaction is strongly ruled by the methylation of the indene, which increases its donor capability, and to a lesser extent by the planarity of the Cp-indene moiety, which finely tunes the donor−acceptor interaction. The oxidation of ferrocene switches on the LMCT absorption in the near-IR region, which is due to an indene-to-ferrocenium electron transfer. The energy and the intensity of the band can be predicted for the oxidation potential of indene relative to that of ferrocene (ΔE). The ΔE values of **1**−**5** reflect all the structural and electronic factors described above. In particular, the degree of redox matching of indene and ferrocene oxidation potentials, which is a requisite for the best efficiency of the donor−acceptor interaction, is increased by methylation, as suggested by the decrease of the energy and the increase of the intensity of the near-IR band. These electrochemical and optical results have been rationalized at the quantum chemistry level by DFT and PCM-TD-DFT calculations.

Our findings represent an important contribution to understanding the main factors ruling the charge transfer process. As recently outlined by Swager,[1a] it is desirable to match the redox potentials of the π-conjugated backbone and the pendant metal

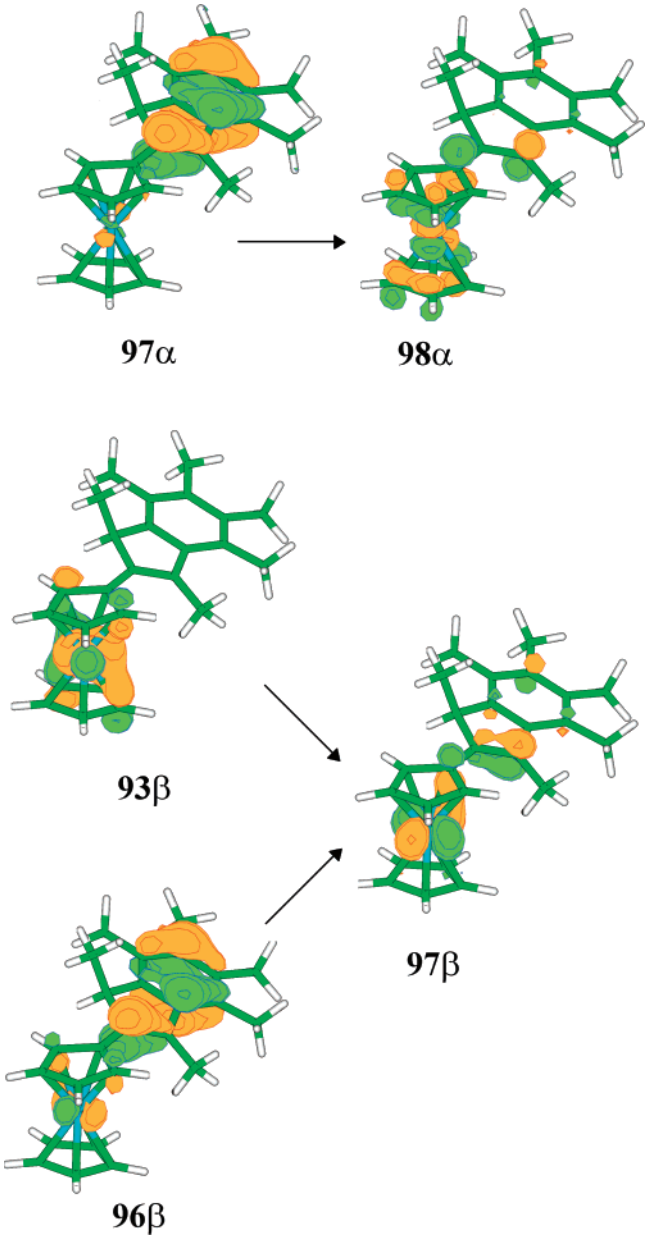

Figure 7. Kohn−Sham molecular spin orbitals involved in the near-IR absorption of $\mathbf{5}^+$ (level: PCM-B3LYP/LANL2DZ,6-31+G*).

group as closely as possible in order to obtain materials with enhanced conductivity, sensory response, and electrocatalytic activity. The challenge is to increase the intensity of the near-IR bands to obtain materials with technological significance.[15c] As for the model ferrocenyl-indene system, we have demonstrated that it is possible to increase the molar absorption coefficients of the near-IR transition by an order of magnitude through "simple" methylation of the π-conjugated hydrocarbon along the series in the order $\mathbf{4}^+ > \mathbf{5}^+ > \mathbf{3}^+ > \mathbf{2}^+ > \mathbf{1}^+$ accompanied by strong red-shift of the band energy.

Experimental Section

General Procedure. All reactions and complex manipulations were performed in an oxygen- and moisture-free atmosphere utilizing standard Schlenk techniques or in a Mecaplex glovebox. Solvents were dried by reflux over the appropriate drying agent and distilled under a stream of argon. Commercial 1,2,3,4-tetramethylbenzene (Sigma-Aldrich) was employed. (3-Ferrocenyl)-indene (**1**) was prepared according to the published procedures. The chromic acid solution (1 L) was prepared partially dissolving $K_2Cr_2O_7$ (17.8 g, 60.5 mmol) in H_2O (200 mL), then adding dropwise H_2SO_4 (13.0 mL, 242 mmol) to the resulting mixture, cooled to 0 °C, and finally H_2O.

Physical Measurements. The X-ray structures were obtained by collecting the intensity data at room temperature using a Philips PW1100 single-crystal diffractometer (FEBO system) using graphite-monochromated (Mo Kα) radiation, following the standard procedures. All intensities were corrected for Lorentz polarization and absorption.[33a] The structure was solved by direct methods using SIR-97.[33b] Refinement was carried out by full-matrix least-squares procedures (based on F_o^2) using anisotropic temperature factors for all non-hydrogen atoms. The H atoms were placed in calculated positions with fixed, isotropic thermal parameters ($1.2U_{equiv}$ of the parent carbon atom). The calculations were performed with the SHELXL-97 program,[33c] implemented in the WinGX package.[33d] HRMS spectra were obtained using an ESI-TOF Mariner 5220 (Applied Biosystem) mass spectrometer with direct injection of the sample and collecting data in the positive mode. IR spectra were recorded on a Bruker Equinox 55 FT-IR spectrometer. ^{1}H and ^{13}C NMR spectra were obtained on a Bruker Avance DRX spectrometer (T = 298 K) operating at 400.13 and 100.61 MHz, respectively. The assignments of the proton resonances were performed by standard chemical shift correlation and NOESY experiments. The ^{13}C resonances were attributed through 2D-heterocorrelated COSY experiments (HMQC[34] using pulsed field gradients for coherence and quadrature detection in F1 achieved by using the TPPI method[34b−d] for the H-bonded carbon atoms, HMBC[34e,f] for the quaternary ones). CV experiments were performed in an airtight three-electrode cell connected to a vacuum/argon line. The reference electrode was a SCE (Tacussel ECS C10) separated from the solution by a bridge compartment filled with the same solvent/supporting electrolyte solution used in the cell. The counter electrode was a platinum spiral with ca. 1 cm^2 apparent surface area. The working electrodes were disks obtained from cross section of gold wires of different diameters (0.5, 0.125, and 0.025 mm) sealed in glass. Between successive CV scans the working electrodes were polished on alumina according to standard procedures and sonicated before use. An EG&G PAR-175 signal generator was used. The currents and potentials were recorded on a Lecroy 9310L oscilloscope. The potentiostat was home-built with a positive feedback loop for compensation of ohmic drop.[35] Mid-IR, near-IR, and visible spectroelectrochemistry experiments at variable temperatures were carried out with a cryostated (low-T) optically transparent thin-layer electrochemical (OTTLE) cell (IDEAS!UvA B.V., University of Amsterdam, The Netherlands)[36] equipped with CaF_2 windows. Pt working (80% transmittance) and Pt auxiliary minigrid electrodes and pseudo-reference Ag wire were

(33) (a) North, A. T. C.; Philips, D. C.; Mathews, F. S. *Acta Crystallogr. A* **1968**, *24*, 351−359. (b) Altomare, A.; Burla, M. C.; Camalli, M.; Cascarano, G. L.; Giacovazzo, C.; Guagliardi, A.; Moliterni, A. G. G.; Polidori, G.; Spagna, R. SIR-97. *J. Appl. Crystallogr.* **1999**, *32*, 115−119. (c) Sheldrick, G. M. *SHELXL-97*, Program for the Refinement of Crystal Structures; University of Göttingen: Germany, 1997. (d) Farrugia, L. J. *J. Appl. Crystallogr.* **1999**, *32*, 837−838.

(34) (a) Bax, A.; Subramanian, S. *J. Magn. Reson.* **1986**, 67, 565−569. (b) Parella, T. *Magn. Reson. Chem.* **1998**, 36, 467−495. (c) Ruiz-Cabello, J.; Vuister, G. W.; Moonen, C. T. W.; van Gelderen, P.; Cohen, J. S.; van. Zijl, P. *J. Magn. Reson.* **1992**, 100, 282−302. (d) Willker, W.; Leibfritz, D.; Kerrsebaum, R.; Bermel, W. *Magn. Reson. Chem.* **1993**, 31, 287−292. (e) Bax, A.; Summers, M. F. *J. Am. Chem. Soc.* **1986**, 108, 2093−2094. (f) Summers, M. F.; Marzilli, L. G.; Bax, A. *J. Am. Chem. Soc.* **1986**, *108*, 4285−4294.

(35) Amatore, C.; Lefrou, C.; Pflüger, F. *J. Electroanal. Chem.* **1989**, *270*, 43−59.

(36) (a) Hartl, F.; Luyten, H.; Nieuwenhuis, H. A.; Schoemaker, G. C. *Appl. Spectrosc.* **1994**, *48*, 1522−1528. (b) Mahabiersing, T.; Luyten, H.; Nieuwendam, R. C.; Hartl, F. *Collect. Czech. Chem. Commun.* **2003**, *68*, 1687−1709.

melt-sealed in the insulating polyethylene spacer with an optical path of 0.019 cm.

Computational Details. Density functional theory (DFT) full geometry optimizations were carried out using the Amsterdam Density Functional (ADF) program.[37] Electron correlation was treated within the local density approximation (LDA) in the Vosko−Wilk−Nusair parametrization,[38] and the nonlocal corrections of Becke[39] and Perdew[40] were added to the exchange and correlation energies. The applied numerical integration procedure was developed by te Velde et al.,[41] and the Hessian matrix update method was implemented by Broyden−Fletcher−Goldfarb−Shanno.[42] The basis sets used for the atoms in the optimization procedures are TZP (triple-ζ Slater-type orbital (STO) basis, extended with a single-z polarization function) frozen core up to 2p for Fe, TZP frozen core up to 1s for C, and TZP for H. Spin contamination in the open-shell calculations was monitored: the expectation value was in all cases very close to the exact value 0.75. TD-DFT calculations were performed by employing the B3LYP hybrid functional and a standard LANL2DZ ECP basis[43] for Fe and 6-31+G*[43] for the other atoms, O, C, and H (this level of theory is denoted in the text as B3LYP/LANL2DZ,6-31+G*), as implemented in the software Gaussian03.[44] This methodological approach was adopted for both neutral and charged species, due to the well-known performance of hybrid functionals in TDDFT calculations. The assignment of the excitation energies to the experimental bands was performed on the basis of the energy values and oscillator strengths; the error falls within the typical range of similar large and open-shell compounds.[13,45] Solvent effects were accounted for using the Polarizable Continuum Model (PCM)[46] in the calculation of the electronic spectra; this level of theory is denoted in the text PCM-TD-DFT. A standard cavity was used, and the dielectric constant of CH_2Cl_2 was 8.93.

Synthesis of (2-Ferrocenyl)indene (2). To a solution of ferrocene (195 mg, 1 mmol) in dry THF (1 mL) was added a pentane solution of *t*-BuLi (1.2 mL, 2 mmol) at 0 °C under argon atmosphere, obtaining a dark orange solution. After stirring for 0.5 h, a solution of $ZnCl_2$ in THF (2.2 mL, 1 mmol) was added. After 0.5 h, the reaction mixture was warmed to 25 °C and stirred for 1 h to give an orange suspension. To the resulting mixture was added a THF solution (3 mL) of 2-bromoindene (200 mg, 1 mmol), followed by the addition of a THF suspension (1 mL) of $PdCl_2(PPh_3)_2$ (24 mg, 0.03 mmol). After stirring for 10 h, the mixture was poured in 15 mL of brine and the organic layer was separated. The water layer was extracted in CH_2Cl_2 (4 × 10 mL). The combined organic layers were dried over anhydrous Na_2SO_4, filtered, concentrated to 2 mL, and eluted on a silica gel column (hexane/CH_2Cl_2, 4:1), yielding **2** as an orange solid (120 mg, 40%). ^{1}H NMR, ^{13}C{^{1}H} NMR, and the analytical data corresponded to those previously reported.[26a,b]

Synthesis of (3-Ferrocenyl)hexamethylindene (3). The intermediate product 2,3,4,5,6,7-hexamethylindan-1-one was prepared according to the procedure previously described.[27b] Complex **3** was prepared by using the same procedure used for the synthesis of **4**. Ferrocene (2.98 g, 16 mmol), *t*-BuLi in pentane (9.41 mL, 16 mmol), and 2,3,4,5,6,7-hexamethylindan-1-one (3.4 g, 15.7 mmol) were used as starting materials for the synthesis of (3-ferrocenyl)-2,3,4,5,6,7-hexamethylindene (2.23 g, 5.8 mmol, 37%). ^{1}H NMR (400.13 MHz, CD_2Cl_2): δ 4.38 (m, 1H, Ha′), 4.37 (m, 1H, Ha), 4.28 (m, 1H, Hb), 4.26 (m, 1H, Hb′), 4.13 (s, 5H, Cp), 3.28 (q, 1H, J(H,CH$_3$) = 7 Hz, H1), 2.46 (s, 3H, 2-CH$_3$), 2.31 (s, 3H, 7-CH$_3$), 2.21 (s, 3H, 6-CH$_3$), 2.14 (s, 3H, 5-CH$_3$), 1.92 (s, 3H, 4-CH$_3$), 1.27 (d, 3H, J(H,CH$_3$) = 7 Hz, 1-CH$_3$). ^{13}C NMR (100.61 MHz, CD_2Cl_2): δ 146.71 (C2), 144.42 (C7a),141.17 (C3a), 134.30 (C5), 132.27 (C3), 130.86 (C6), 127.94 (C7), 126.33 (C4), 84.91 (Cj), 71.43 (Ca), 71.29 (Ca′), 69.32 (CCp), 66.74 (Cb), 66.46 (Cb′), 47.60 (C1), 19.03 (4-CH$_3$), 16.57 (1-CH$_3$), 16.42 (7-CH$_3$), 16.10 (5-CH$_3$), 15.77 (6-CH$_3$), 14.94 (2-CH$_3$). HRMS (ESI$^+$): *m*/*z* calcd for $C_{25}H_{28}Fe$ (M^+), 384.1535; found, 384.1414. Anal. Calcd for $C_{25}H_{28}Fe$: C, 78.13; H, 7.34. Found: C, 77.84; H, 7.51.

Synthesis of (2-Ferrocenyl)tetramethylindene (4). Preparation of 4,5,6,7-Tetramethylindene. The synthesis of 4,5,6,7-tetramethylindene was previously reported.[47] Here we report an alternative method and a more detailed characterization. The intermediate product 4,5,6,7-tetramethylindan-1-one was prepared with a method similar to that previously described by R. B. Woodward et al.[48] for the synthesis of *s*-hydrindacen-1-one. 1,2,3,4-Tetramethylbenzene (10.8 g, 80.4 mmol), $AlCl_3$ (40.4 g, 303 mmol), β-chloropropionyl chloride (7.4 mL, 89.9 mmol), and 80 mL of CH_3NO_2 were used as starting materials. A crude brown oil of 3-chloro-1-(2,3,4,5-tetramethylphenyl)propan-1-one was obtained and subsequently treated with H_2SO_4 (108 mL) to give the crude ketone. Purification on a silica gel column using petroleum ether/diethyl ether (9:1) as eluent gave 4,5,6,7-tetramethylindan-1-one (7.57 g, 40.0 mmol, 50%) as a white powder. Lithium aluminum hydride (26 mL, 1 M in THF, 26 mmol) was dissolved under argon in 100 mL of dry THF in a 500 mL three-necked flask equipped with a pressure-equalized dropping funnel, reflux condenser, and stirrer bar. With vigorous stirring the reaction mixture was cooled to 0 °C, and a solution of 4,5,6,7-tetramethylindan-1-one (4.02 g, 21.2 mmol) in 90 mL of dry THF was transferred by cannula to the dropping funnel and added dropwise to the reaction vessel over 15 min. The resulting solution was refluxed for 4 h and cooled to 0 °C. Then, ethyl acetate (5 mL), 5% aqueous THF (20 mL), water (20 mL), and 10% aqueous HCl (25 mL) were slowly added. The reaction mixture was extracted in $CHCl_3$ (4 × 60 mL), and the combined organic layers were washed with water (50 mL), saturated $NaHCO_3$ aqueous solution of (2 × 50 mL), water (2 × 50 mL), and saturated NaCl aqueous solution (25 mL), and dried over anhydrous Na_2-

(37) (a) te Velde, G.; Bickelhaupt, F. M.; van Gisbergen, S. J. A.; Fonseca Guerra, C.; Baerends, E. J.; Snijders, J. G.; Ziegler, T. Chemistry with ADF. *J. Comput. Chem.* **2001**, *22*, 931−967. (b) Fonseca Guerra, C.; Snijders, J. G.; te Velde, G.; Baerends, E. J. *Theor. Chem. Acc.* **1998**, *99*, 391−403. (c) *ADF 2006.01*; SCM, Theoretical Chemistry, Vrije Universiteit, Amsterdam, The Netherlands, http://www.scm.com.

(38) Vosko, S. D.; Wilk, L.; Nusair, M. *Can. J. Chem.* **1990**, *58*, 1200−1211.

(39) (a) Becke, A. D. *J. Chem. Phys.* **1986**, *84*, 4524−4529. (b) Becke, A. D. *Phys. Rev. A* **1988**, *38*, 3098−3100.

(40) (a) Perdew, J. P. *Phys. Rev. B* **1986**, *33*, 8822−8824. (b) Perdew, J. P. *Phys. Rev. B* **1986**, *34*, 7406.

(41) te Velde, G.; Baerends, E. J. *J. Comput. Phys.* **1992**, *99*, 84−98.

(42) (a) Broyden, C. G. *IMA J. Math. Appl.* **1970**, *6*, 222−231. (b) Fletcher, R. *Comput. J.* **1970**, *13*, 317−322. (c) Goldfarb, D. *Math. Comput.* **1970**, *24*, 23−26. (d) Shanno, D. F. *Math. Comput.* **1970**, *24*, 647−656.

(43) Basis sets were obtained from the Extensible Computational Chemistry Environment Basis Set Database, Version 02/25/04, as developed and distributed by the Molecular Science Computing Facility, Environmental and Molecular Sciences Laboratory, which is part of the Pacific Northwest Laboratory, P.O. Box 999, Richland, Washington 99352, and funded by the U.S. Department of Energy. The Pacific Northwest Laboratory is a multiprogram laboratory operated by Battelle Memorial Institute for the U.S. Department of Energy under contract DE-AC06-76RLO 1830. (a) Hay, P. J.; Wadt, W. R. *J. Chem. Phys.* **1985**, *82*, 270−283. (b) Hay, P. J.; Wadt, W. R. *J. Chem. Phys.* **1985**, *82*, 284−298. (c) Hay, P. J.; Wadt, W. R. *J. Chem. Phys.* **1985**, *82*, 299−310.

(44) Frisch, M. J.; et al. *Gaussian 03*, Revision C.02; Gaussian, Inc.: Wallingford, CT, 2004.

(45) (a) Wang, F.; Ziegler, T. *Mol. Phys.* **2004**, *102*, 2585−2595. (b) Medei, L.; Orian, L.; Semeikin, O. V.; Peterleitner, M. G.; Ustynyuk, N. A.; Santi, S.; Durante, C.; Ricci, A.; Lo Sterzo, C. *Eur. J. Inorg. Chem.* **2006**, *13*, 2582−2597. (c) Cotton, F. A.; Liu, C. Y.; Murillo, C. A.; Villagran, D.; Wang, X. P. *J. Am. Chem. Soc.* **2004**, *126*, 14822−14831.

(46) (a) Cances, M. T.; Mennucci, B.; Tomasi, J. *J. Chem. Phys.* **1997**, *107*, 3032−3041. (b) Cossi, M.; Barone, V.; Mennucci, B.; Tomasi, J. *Chem. Phys. Lett.* **1998**, *286*, 253−260. (c) Mennucci, B.; Tomasi, J. *J. Chem. Phys.* **1997**, *106*, 5151−5158. (d) Cossi, M.; Scalmani, G.; Rega, N.; Barone, V. *J. Chem. Phys.* **2002**, *117*, 43−54.

(47) Ready, T. E.; Chien, J. C. W.; Rausch, M. D. *J. Organomet. Chem.* **1999**, *583*, 11−27.

(48) Woodward, R. B.; Hoye, T. R. *J. Am. Chem. Soc.* **1977**, *99*, 8007−8014.

SO_4. The solvent was removed under vacuum and the residue washed with pentane, yielding a white powder of 4,5,6,7-tetramethylindan-1-ol (3.45 g,18.0 mmol, 85%). In a 1 L round-bottom flask fitted with a stirrer bar and reflux condenser 4,5,6,7-tetramethylindan-1-ol (3.0 g, 15.7 mmol) was dissolved in 600 mL of anhydrous toluene. A catalytic amount of *p*-toluenesulfonic acid (0.15 g, 0.79 mmol) was added and the solution warmed to 65 °C for 2 h. After cooling to room temperature, the mixture was washed with H_2O (3 × 300 mL) and saturated NaCl aqueous solution (2 × 240 mL) and dried over anhydrous Na_2SO_4. After filtration, the solvent was removed under vacuum and the residue eluted on a silica gel column using petroleum ether as eluent. The final product 4,5,6,7-tetramethylindene (2.45 g, 14.2 mmol, 90%) was obtained as a white stable solid. ^{1}H NMR (400.13 MHz, CD_2Cl_2, δ ppm, 298 K, TMS): δ 6.99 (m, 1H, H3), 6.46 (m, 2H, H2), 3.30 (m, 2H, H1), 2.35 (s, 3H, 4-CH_3), 2.27 (s, 3H, 7-CH_3), 2.24 (s, 3H, 5-CH_3), 2.23 (s, 3H, 6-CH_3). ^{13}C NMR (100.61 MHz, CD_2Cl_2, δ ppm, 298K, TMS): δ 140.42 (C3a), 139.40 (C7a), 132,55 (C4),-131.62 (C2), 131.07 (C6), 130.70 (C3), 128.40 (C7), 125.61 (C5), 38.53 (C1), 15.91 (7-CH_3), 15.59 (4-CH_3), 15.41 (5-CH_3), 15.34 (6-CH_3). Anal. Calcd for $C_{13}H_{16}$: C, 90.63; H, 9.37. Found; C, 90.42; H, 9.58.

Preparation of 4,5,6,7-Tetramethylindan-2-one. Hydroboration−oxidation with diborane (12.7 mL, 1 M in THF, 12.7 mmol) in THF (15 mL) for the conversion of 4,5,6,7-tetramethylindene (2.2 g, 12.7 mmol) to the corresponding 4,5,6,7-tetramethylindan-2-ol was performed according to the method described for the indene by P. A. Marshall et al.[49] The workup procedure consisted in the addition of diethyl ether (130 mL) to the reaction mixture, which was then washed with water (2 × 70 mL) and saturated NaCl aqueous solution (2 × 70 mL) and dried over anhydrous Na_2SO_4. After filtration, the solvent was removed under vacuum and the residue washed with small portions of pentane to give a mixture of 4,5,6,7-tetramethylindan-2-ol/4,5,6,7-tetramethylindan-1-ol (2.31 g, 16:1) as a white powder. In a 500 mL round-bottom flask fitted with a stirrer bar and reflux condenser the mixture was dissolved in ether (150 mL). Chromic acid solution (2 × 66 mL) was added under vigorous stirring to the solution cooled at −5 °C. The biphasic reaction mixture was warm to 30 °C, and after 4 h a chromic acid solution (66 mL) was added for the third time. Vigorous stirring at 30 °C was maintained overnight. Twenty hours after the first addition of oxidant agent the dark green aqueous phase was removed by cannula and replaced with fresh chromic acid solution (66 mL). Four hours later the reaction mixture was cooled to room temperature, the aqueous layer was extracted in diethyl ether (4 × 60 mL), and the combined organic layers were washed with an aqueous solution of Na_2CO_3 (1 M, 4 × 80 mL), water (3 × 60 mL), and a saturated aqueous solution of NaCl (120 mL) and dried over anhydrous Na_2SO_4. After filtration, the solvent was removed under vacuum and the residue eluted on a silica gel column using petroleum ether/diethyl ether (4:1) as eluent to give 4,5,6,7-tetramethylindan-2-one (0.58 g, 3.1 mmol, yield 24% with respect to 4,5,6,7-tetramethylindene) as a white solid. The characterization of 4,5,6,7-tetramethylindan-2-one was previously reported.[50] Complex **4** was finally prepared according to the literature:[26b] ferrocene (0.52 g, 2.8 mmol), a pentane solution of *t*-BuLi (1.64 mL, 12.8 mmol), and 4,5,6,7,-tetramethylindan-2-one (0.5 g, 2.7 mmol) were used as starting materials. After purification of the crude product on a silica gel column using petroleum ether/diethyl ether (95:5) as eluent, complex **4** (0.167 g, 0.47 mmol, yield 17%) was obtained as an orange stable solid. ^{1}H NMR (400.13 MHz, CD_2Cl_2): δ 6.92 (m, 1H, H3), 4.56 (m, 2H, Ha,Ha′), 4.30 (m, 2H, Hb,Hb′), 4.08 (s, 5H, Cp), 3.56 (m, 2H, H1), 2.33 (s, 3H, 4-CH_3), 2.31 (s, 3H, 7-CH_3), 2.23 (s, 6H, 5-CH_3, 6-CH_3). ^{13}C NMR (100.61 MHz, CD_2Cl_2): δ 144.34 (C2), 142.22 (C7a), 139.05 (C3a), 133.51 (C4), 131.15 (C6), 128.85 (C7), 125.35 (C5), 123.54 (C3), 82.23 (Cj), 69.73 (CCp), 69.20 (Cb, Cb′), 66.50 (Ca, Ca′), 40.00 (C1), 16.64 (7-CH_3), 16.31 (4-CH_3), 16.13 (5-CH_3, 6-CH_3). HRMS (ESI$^+$): *m*/*z* calcd for $C_{23}H_{24}Fe$ (M^+), 356.1222; found, 356.1139. Anal. Calcd for $C_{23}H_{24}$-Fe: C, 77.54; H, 6.79. Found: C, 77.02; H, 6.93.

Synthesis of (2-Ferrocenyl)hexamethylindene (5). Preparation of 1,3,4,5,6,7-Hexamethylindene. To the stirring mixture of $AlCl_3$ (38.2 g, 286 mmol) in CS_2 (150 mL) at −5 °C was slowly added a mixture of 1,2,3,4-tetramethylbenzene (26.0 g, 194 mmol) and *trans*-crotonyl chloride (18.8 mL, 195 mmol) in 1 h. The orange mixture was warmed to room temperature and stirred overnight. It was then heated at 50 °C for 2 h and finally poured onto ice (400 g) and concentrated HCl (400 mL). The mixture was then extracted in diethyl ether and the ether layer dried over Na_2SO_4. The solvent was removed under vacuum and the crude yellow solid washed with small portion of pentane, affording 3,4,5,6,7-tetramethylindan-1-one (24.93 g, 123.2 mmol, yield 64%).

A suspension of Mg (4.5 g, 185 mmol) in diethyl ether (33 mL) in a three-necked flask equipped with two pressure-equalized dropping funnels, reflux condenser, and stirrer bar was maintained under vigorous stirring for 5 min. A solution of CH_3I (30 g, 211 mmol) in 23 mL of diethyl ether was slowly added, and then the mixture was refluxed over a period 1 h. To the resulting gray mixture cooled to −5 °C was added dropwise a solution of 3,4,5,6,7-pentamethylindan-1-one (22.2 g, 110 mmol) in 250 mL of diethyl ether. The obtained mixture was refluxed again for 2.5 h and then cooled to −5 °C. Water (88 mL) was added followed by dropwise addition of concentrated HCl (44 mL). Vigorous stirring was maintained overnight. The aqueous layer was extracted in diethyl ether (4 × 100 mL), and the combined organic layers were washed with an aqueous solution of $Na_2S_2O_3$ (0.3 M, 4 × 100 mL), water (2 × 100 mL), and a NaCl-saturated aqueous solution (2 × 100 mL) and dried over anhydrous Na_2SO_4. After filtration, the solvent was removed under vacuum and the residue eluted on a silica gel column using petroleum ether as eluent to give the final product 1,3,4,5,6,7-hexamethylindene (14.3 g, 71.4 mmol, 65%) as white stable solid. ^{1}H NMR (400.13 MHz, $CDCl_3$): δ 6.05 (s, 1H, H2), 3.42 (q, 1H, J(H,CH_3) = 7 Hz, H1), 2.51 (s, 6H, 4-CH_3, 7-CH_3), 2.36 (s, 3H, 3-CH_3), 2.27 (s, 6H, 5-CH_3, 6-CH_3), 1.26 (d, 3H, J(H,-CH_3) = 7 Hz, 1-CH_3).^{13}C NMR (100.61 MHz, $CDCl_3$): δ 146.50 (C3a), 139.73 (C1a), 139.16 (C3), 137.84 (C2), 133.84 (C5), 131.95 (C4), 129.99 (C7), 127.38 (C6), 42.18 (C1), 18.81 (3-CH_3), 16.31 (1-CH_3, 5-CH_3, 6-CH_3), 15.66 (4-CH_3, 7-CH_3). Anal. Calcd for $C_{15}H_{20}$: C, 89.94; H, 10.06. Found: C, 89.95; H, 10.26.

Preparation of 1,3,4,5,6,7-Hexamethylindan-2-one. The intermediate product 1,3,4,5,6,7-hexamethylindan-2-ol was prepared following the same procedure utilized for the preparation of 4,5,6,7-tetramethylindan-2-ol described above. On reacting 1,3,4,5,6,7-hexamethylindene (11.0 g, 55.0 mmol) with a THF solution of diborane (100 mL, 50.0 mmol), we obtained 1,3,4,5,6,7-hexamethylindan-2-ol (9.6 g, 44 mmol, yield 80%). 1,3,4,5,6,7-Hexamethylindan-2-one was obtained by oxidation with chromic acid following the same procedure described for 4,5,6,7-tetramethylindan-2-one. The reaction of 1,3,4,5,6,7-hexamethylindan-2-ol (4.4 g, 20.1 mmol) with chromic acid solution (4 × 108 mL) in diethyl ether (240 mL) gave 1,3,4,5,6,7-hexamethylindan-2-one (1.74 g, 8.04 mmol, yield 40%) as a white stable solid. ^{1}H NMR (400.13 MHz, $CDCl_3$): δ 3.45 (q, 2H, J(H,CH_3) = 7 Hz, H1, H3), 2.25 (s, 6H, 5-CH_3, 6-CH_3), 2.24 (s, 6H, 4-CH_3, 7-CH_3), 1.44 (d, 6H, J(H,-CH_3) = 7 Hz, 1-CH_3, 3-CH_3). ^{13}C NMR (100.61 MHz, $CDCl_3$): δ 222.38 (C2), 138.18 (C1a, C3a), 134.59 (C4, C7), 129.82 (C5, C6), 47.73 (C1, C3), 19.31 (1-CH_3, 3-CH_3), 16.32 (4-CH_3, 7-CH_3), 16.05 (5-CH_3, 6-CH_3). Anal. Calcd for $C_{15}H_{20}O$: C, 83.27; H, 9.32. Found: C, 82.81; H, 9.58.

Finally, complex **5** was prepared using the same procedure described for **4**. The reaction of 1,3,4,5,6,7,-hexamethylindan-2-

(49) Marshall, P. A.; Prager, R. H. *Aust. J. Chem.* **1979**, *32*, 1251−1260.

(50) Heldeweg, R. F.; Hogeveen, H. *J. Am. Chem. Soc.* **1976**, *98*, 6040−6042.

one (1.0 g, 4.6 mmol with ferrocene (0.876 g, 4.7 mmol) and *t*-BuLi (2.77 mL, 1.7 M in pentane, 4.7 mmol) gave 1,3,4,5,6,7-hexamethyl-2-Fc-indan-2-ol (0.608 g, 1.51 mmol, 33%) as a yellow stable solid. The latter (0.5 g, 1.24 mmol) was dissolved under argon in 150 mL of anhydrous toluene, a catalytic amount of *p*-toluenesulfonic acid (10 mg, 0.052 mmol) was added, and the resulting solution was stirred at room temperature for 5 h. Subsequently the mixture was washed with an aqueous solution of $NaHCO_3$ (3 × 50 mL), dried over anhydrous Na_2SO_4, and filtered. The solvent was removed under vacuum to give **5** (0.457 g, 1.19 mmol, 96%). Crystals suitable for X-ray analysis were grown from slow diffusion of *n*-pentane into a CH_2Cl_2 solution at −30 °C. ^{1}H NMR (400.13 MHz, CD_2Cl_2): δ 4.51 (m, 1H, Ha), 4.47 (m, 1H, Ha′), 4.32 (m, 2H, Hb, Hb′), 4.11 (s, 5H, Cp), 3.57 (q, 1H, J(H,-CH_3) = 7 Hz, H1), 2.60 (s, 3H, 3-CH_3), 2.53 (s, 3H, 4-CH_3), 2.32 (s, 3H, 7-CH_3), 2.25 (s, 3H, 5-CH_3), 2.23 (s, 3H, 6-CH_3), 1.15 (d, 3H, J(H,CH_3) = 7 Hz, 1-CH_3). ^{13}C NMR (100.61 MHz, CD_2Cl_2): δ 145.14 (C7a), 143.43 (C2),140.93 (C3a), 133.74 (C5), 133.37 (C3), 131.12 (C6), 127.78 (C7), 126.51 (C4), 81.39 (Cj), 69.35 (Ca), 69.21 (Cb′), 68.95 (CCp), 67.94 (Cb), 67.68 (Ca′), 44.95 (C1), 17.53 (1-CH_3), 16.89 (3-CH_3), 16.11 (6-CH_3), 16.03 (4-CH_3), 15.86 (5-CH_3), 16.47 (7-CH_3). HRMS (ESI$^+$): *m*/*z* calcd for $C_{25}H_{28}Fe$ (M^+), 384.1535; found, 384.1389. Anal. Calcd for $C_{25}H_{28}Fe$: C, 78.13; H, 7.34. Found: C, 77.82; H, 7.46.

Synthesis of Tetrafluoroborate Salts of Cations 1^+−5^+. A typical preparation follows.

[4][BF_4]. Solid $AgBF_4$ (13.7 mg, 0.07 mmol) was added to a stirred solution of **4** (25 mg, 0.07 mmol) in diethyl ether (20 mL) at room temperature. After 0.5 h the solvent was removed under vacuum and the residue extracted in CH_2Cl_2 (5 mL). After filtration through Celite, the volume of the dark extract was reduced under vacuum to ca. 1 mL, and diethyl ether (50 mL) was added. The dark red precipitate was then further purified from CH_2Cl_2/diethyl ether to give [**4**][BF_4] (21.5 mg, 0.048 mmol, 68%). HRMS (ESI$^+$): *m*/*z* calcd for $C_{23}H_{24}Fe$ (M^+), 356.1222; found, 356.1215. Anal. Calcd for $C_{23}H_{24}FeBF_4$: C, 62.34; H, 5.46. Found: C, 62.13; H, 5.31.

[1][BF_4]. From **1** (60 mg, 0.20 mmol) and $AgBF_4$ (38.9 mg, 0.2 mmol): 24 mg, 0.062 mmol, 31%. HRMS (ESI$^+$): *m*/*z* calcd for $C_{19}H_{16}Fe$ (M^+), 300.0596; found, 300.0665. Anal. Calcd for $C_{19}H_{16}FeBF_4$: C, 58.97; H, 4.17. Found: C, 58.62; H, 4.06.

[2][BF_4]. From **2** (90 mg, 0.3 mmol) and $AgBF_4$ (58.4 mg, 0.3 mmol): 75 mg, 0.19 mmol, 63%. HRMS (ESI$^+$): *m*/*z* calcd for $C_{19}H_{16}Fe$ (M^+), 300.0596; found, 300.0645. Anal. Calcd for $C_{19}H_{16}FeBF_4$: C, 58.97; H, 4.17. Found: C, 58.79; H, 4.29.

[3][BF_4]. From **3** (50 mg, 0.13 mmol) and $AgBF_4$ (25.3 mg, 0.13 mmol): 22 mg, 0.047 mmol, 36%. HRMS (ESI$^+$): *m*/*z* calcd for $C_{25}H_{28}Fe$ (M^+), 384.1535; found, 384.1058. Anal. Calcd for $C_{25}H_{28}FeBF_4$: C, 63.73; H, 5.99. Found: C, 63.32; H, 6.12.

[5][BF_4]. From **5** (90 mg, 0.23 mmol) and $AgBF_4$ (45 mg, 0.23 mmol): 58 mg, 0.12 mmol, 52%. HRMS (ESI$^+$): *m*/*z* calcd for $C_{25}H_{28}Fe$ (M^+), 384.1535; found, 384.1381. Anal. Calcd for $C_{25}H_{28}FeBF_4$: C, 63.73; H, 5.99. Found: C, 63.22; H, 6.02.

Acknowledgment. This work was supported by the Ministero dell'Università e della Ricerca (MUR) within PRAT 2006. CINECA (Consorzio di calcolo del Nord-Est, Casalecchio di Reno) is greatly acknowledged for the generous allocation of computational time on the IBM-SP5. We wish to gratefully acknowledge Mr. Samuele Zanatta for ESI-MS analysis.

Supporting Information Available: Cartesian coordinates of all the neutral and charged complexes; Kohn−Sham frontier molecular orbitals of the neutral and charged optimized complexes $\mathbf{1}^{0/+1}$−$\mathbf{5}^{0/+1}$ (level: ZORA/TZP small frozen core); Kohn−Sham selected frontier molecular orbitals of the neutral and charged optimized complexes $\mathbf{1}^{0/+1}$−$\mathbf{5}^{0/+1}$ (level: PCM-B3LYP/LANL2DZ,6-31+G*); complete ref 43. This material is available free of charge via the Internet at http://pubs.acs.org.

OM700673M